Assessment of a smart concept for d_{15} shear piezoceramic direct torsion actuation

Ayech Benjeddou

Institut Supérieur de Mécanique de Paris
Supméca Structures
F-93407 Saint Ouen cedex
benjeddou@supmeca.fr

ABSTRACT. *An experimentally proved smart concept for piezoceramic direct torsion actuation is here numerically assessed with regards to the bonding and segmentation influence on its behavior and performance. The TRESCA and deflection criteria analysis indicates that the actuator sandwiching with composites contributes to its integrity enhancement, but in the cost of its performance reduction. It is also found that modeling the core inter-rows and composites inter-layers bonding is more influential than that of the core rows segmentation. The conducted open-circuit modal analysis confirms that the inter-rows adhesive softens the actuator, while the inter-layers one stiffens it. Besides, the conducted adhesive parametric analysis indicates that, as expected, the most influential bonding parameters are its thickness and shear modulus.*

RÉSUMÉ. *Un concept intelligent, prouvé expérimentalement, pour l'action piézocéramique directe en torsion est ici évalué numériquement par rapport à l'influence du collage et de la segmentation sur son comportement et sa performance. L'analyse des critères de TRESCA et de la flèche indique que la mise en sandwich de l'actionneur par des composites contribue à l'amélioration de son intégrité, mais au prix de la réduction de sa performance. Il est aussi montré que la modélisation du collage entre les rangées du cœur et les couches composites est plus influente que celle de la segmentation du cœur. L'analyse modale effectuée en court-circuit confirme que la colle entre rangées assouplit l'actionneur, alors que celle entre les couches le rigidifie. De plus, L'analyse paramétrique de la colle indique que, comme prévu, les paramètres du collage les plus influents sont son épaisseur et son module de cisaillement.*

KEYWORDS: *direct torsion actuation smart concept, piezoelectric d_{15}-shear response, bonding, segmentation, open-circuit modal analysis, bonding parametric analysis.*

MOTS-CLÉS : *concept intelligent d'action directe en torsion, réponse piézoélectrique en cisaillement d_{15}, collage, segmentation, analyse modale en circuit-ouvert, analyse paramétrique du collage.*

DOI:10.3166/EJCM.20.103-124

1. Introduction

The use of composite materials in many industries has rapidly grown during the last decade; this is particularly noticeable for flexible space structures, aircrafts and turbines. Nevertheless, they are often subjected to torsion vibration, which control is a critical issue for some of their vital components such as wings and blades. Fortunately, modern composite structures allow the integration of the smart materials, such as piezoceramic ones, for their torsion control. Torsion actuation can be induced indirectly, using piezoceramic patches, for angle-ply laminated composite structures, that present bending-twist or extension-twist mechanical couplings, or for other composite structures using oriented piezoceramic fibers or skewed piezoelectric patches; see the review (Chopra 2002), and (Tzou *et al.*, 2008) for a recent concept. Torsion actuation can be also obtained directly via the piezoelectric coupling constant d_{36}; unfortunately, although it is non nil for materials of crystal symmetry 4mm, like ADP (Zehetner 2009), it is nil for the popular piezoelectric polymers, which are of crystal symmetry 2mm, and piezoceramic materials, which are of crystal symmetry 6mm (IEEE 1988). An alternative solution for the latter is to use their shear response via the piezoelectric coupling constant d_{15}; unfortunately, piezoelectric polymers, like the popular PVDF material, have nil d_{15} shear response (Benjeddou 2007). Hence, torsion actuation was induced experimentally by assembling circumferentially-polarized *tubular* piezoceramic segments (Centolanza *et al.*, 2002; Powar *et al.*, 2008) and, theoretically, using *width*-polarized bimorphs (Thakkar *et al.*, 2004) and using two *length*-oppositely polarized (OP) long and thick PZT-5H patches (Butz *et al.*, 2008).

Recently, the theoretical direct torsion actuator (Butz *et al.*, 2008) has been made realistic, in dimensions and actuation voltage, so that it can be manufactured and used in practice; then, it has been sandwiched between composite faces and experimentally proved (Berik *et al.*, 2010). The resulting smart concept consists now of two OP rows of three d_{15} shear PIC255 patches with length-same polarizations (SP). Notice that the present torsion actuation mechanism (TAM) has to be used, like for the so-called shear actuation mechanism (Benjeddou 2007), as a core sandwiched between elastic faces so that it can be transversely sheared. Its design-dependent behavior and performance are here assessed numerically via its three-dimensional (3D) finite element (FE) analysis using ABAQUS® commercial code. Focus is made on the evaluation of the adhesives and segmentation influence on the piezoceramic basic and smart composite actuators behavior and performance. For this purpose, various FE models, with increasing complexity regarding the adhesives and segmentation modeling, of the present smart concept are proposed and analyzed. Besides, in order to detect potential critical zones at the different interfaces, attention is paid to the shear stresses concentrations and displacements distributions by analyzing the distributions of the TRESCA stress and transverse displacement that can be post-processed for effective rate of twist evaluation (Berik *et al.*, 2010); Moreover, open-circuit modal and bonding parametric analyses are conducted before the traditional conclusions and perspectives closure section.

2. Piezoceramic shear-induced torsion actuation mechanism

The 3D linear *converse* constitutive equation, that governs the *actuation* response using a piezoceramic material (isotropic transverse) having its *polarization lying conventionally along the material axis 3*, can be written in this *e-form* which is implemented in the classical displacement-potential finite elements of commercial codes, like ABAQUS® for example

$$\begin{Bmatrix} T_1 \\ T_2 \\ T_3 \\ T_4 \\ T_5 \\ T_6 \end{Bmatrix} = \begin{bmatrix} C_{11}^E & C_{12}^E & C_{13}^E & 0 & 0 & 0 \\ C_{12}^E & C_{11}^E & C_{13}^E & 0 & 0 & 0 \\ C_{13}^E & C_{13}^E & C_{33}^E & 0 & 0 & 0 \\ 0 & 0 & 0 & C_{55}^E & 0 & 0 \\ 0 & 0 & 0 & 0 & C_{55}^E & 0 \\ 0 & 0 & 0 & 0 & 0 & C_{66}^E = \frac{1}{2}(C_{11}^E - C_{12}^E) \end{bmatrix} \begin{Bmatrix} S_1 \\ S_2 \\ S_3 \\ S_4 \\ S_5 \\ S_6 \end{Bmatrix} - \begin{bmatrix} 0 & 0 & e_{31} \\ 0 & 0 & e_{31} \\ 0 & 0 & e_{33} \\ 0 & e_{15} & 0 \\ e_{15} & 0 & 0 \\ 0 & 0 & 0 \end{bmatrix} \begin{Bmatrix} E_1 \\ E_2 \\ E_3 \end{Bmatrix} \quad [1]$$

where, T_p (p=1,…,6) are the Cauchy stresses; S_p, are the linearized strains; E_k (k=1,2,3), are the electric fields; C_{pq}^E , e_{3k} (q=1,…,6) are the elastic constants (N/m^2) at constant electric field, and stress piezoelectric constants (C/m^2).

For a piezoceramic patch with electroded major surfaces, as shown in Figure 1, the transverse electric field component E_1 dominates the other ones, and the electric (e) field – induced *actuation stress* vector (right part only of above equation) is

$$\begin{Bmatrix} T_1 \\ T_2 \\ T_3 \\ T_4 \\ T_5 \\ T_6 \end{Bmatrix}^e = - \begin{bmatrix} 0 & 0 & e_{31} \\ 0 & 0 & e_{31} \\ 0 & 0 & e_{33} \\ 0 & e_{15} & 0 \\ e_{15} & 0 & 0 \\ 0 & 0 & 0 \end{bmatrix} \begin{Bmatrix} E_1 \\ 0 \\ 0 \end{Bmatrix} = \begin{Bmatrix} 0 \\ 0 \\ 0 \\ 0 \\ -e_{15} E_1 \\ 0 \end{Bmatrix} \quad [2]$$

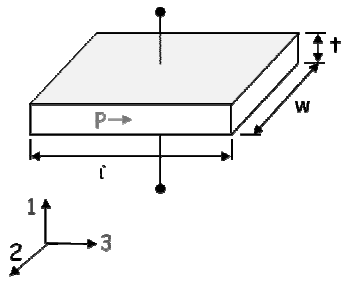

Figure 1. *Lengthwise-polarized piezoceramic patch with electroded major surfaces*

Now, consider the left side-clamped (cantilever) actuator shown in Figure 2 which is adapted from the theoretical benchmark given in (Butz *et al.*, 2008); it consists of two piezoceramic patches that are assembled in lengthwise-OP. After rotating above patch (Figure 1) +90° around the 3-axis, the lower patch which has a *positive poling* (along + x-axis of the global frame system) will induce electrically the following actuation stress vector in the Cartesian (global) frame system

$$\begin{Bmatrix} \sigma_{xx} \\ \sigma_{yy} \\ \sigma_{zz} \\ \sigma_{yz} \\ \sigma_{xz} \\ \sigma_{xy} \end{Bmatrix}^{e} = -\begin{bmatrix} e_{11} & 0 & 0 \\ e_{12} & 0 & 0 \\ e_{13} & 0 & 0 \\ 0 & 0 & 0 \\ 0 & 0 & e_{35} \\ 0 & e_{26} & 0 \end{bmatrix} \begin{Bmatrix} 0 \\ 0 \\ E_z \end{Bmatrix} = -\begin{bmatrix} e_{33} & 0 & 0 \\ e_{31} & 0 & 0 \\ e_{31} & 0 & 0 \\ 0 & 0 & 0 \\ 0 & 0 & e_{15} \\ 0 & e_{15} & 0 \end{bmatrix} \begin{Bmatrix} 0 \\ 0 \\ E_z \end{Bmatrix} = \begin{Bmatrix} 0 \\ 0 \\ 0 \\ 0 \\ -e_{15}E_z \\ 0 \end{Bmatrix} \qquad [3]$$

The upper patch which has a *negative poling* (along – x-axis of the global frame system) will induce, after rotating above patch (Figure 1) by +90° around the 3-axis, followed by +180° around the 2-axis, an opposite electrical actuation shear stress of $\sigma_{xz} = e_{15}E_z$ is obtained, where double indices notation is used for the Cartesian stresses in order to distinguish them from the local ones in Equation [2].

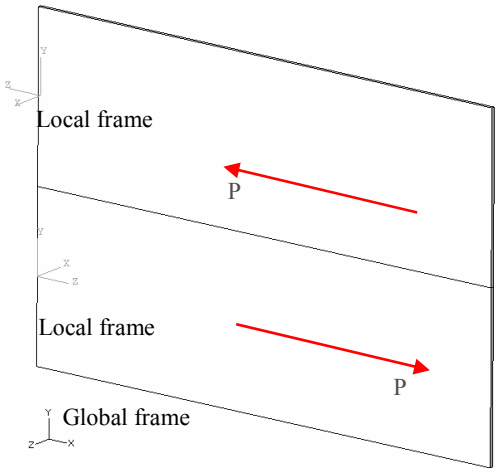

Figure 2. *Left side clamped actuator assembled from two OP piezoceramic patches*

After the integration of these electrically-induced actuation shear stresses over the two patches y-z cross-sections, the resulting shear stress resultants are along the Cartesian – z-axis and + z-axis for the lower and upper patches, respectively; since $e_{15}>0$ and assuming that the applied electric field E_z is constant and has a positive

value, this creates a torsion moment that deforms the actuator in torsion as illustrated in Figure 3. Hence, the bottom layer of the actuator should deform the actuator negatively along the z-direction, while the top layer should deform it positively to this direction; the combination of these deformations should produce a global torsion of the cantilevered actuator because the patches are identical (have the same shear modulus) and the transverse shear stress σ_{xz} should be continuous at the bottom/top patches interface; the latter is the location of the neutral and torsion axes due to the construction symmetry; hence, it should not move transversely as confirmed by Figure 3 (see the zero deflection at the patches interface), which results from the Figure 2 FE simulation using the basic model as explained later.

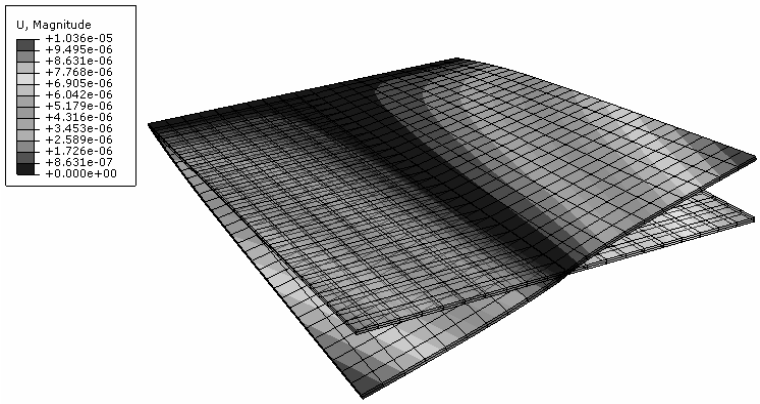

Figure 3. *The basic actuator deformation under 198V static torsion actuation (Figure 2 basic model as detailed later)*

Notice that the local frame system of the lower patch of Figure 2 has to be +90° clockwise rotated around its y-axis, while that of the upper patch has to be -90° anti-clockwise rotated around the same y-axis, in order to coincide with those of the actuator global frame system. These rotations are to be made in order to avoid local frames–based implementation of the OP. Indeed, an alternative technique is to use two data sets, where one of them implements the negative poling simply by adding a minus sign before the piezoelectric coupling constants (Chevallier *et al*., 2009).

3. Assessment of the basic torsion actuator

The direct torsion actuator, proposed in (Butz *et al*., 2008) as a theoretical benchmark for a 3D piezoelectric beam FE model, is shown in Figure 4a. It consists of two OP d_{15} shear PZT-5H patches. The used thickness of 2mm is the maximum available commercially; however, the used length of 100mm is not commercially available (maximum in-plane dimension is 25mm). The applied electric potentials of

1000V (too high) on the +z electroded face and 0V on the opposite one provide an actuation electric field of 500V/mm. This theoretical concept has been recently made realistic, in dimension and actuation voltage, so that it can be experimentally proved and used in practice (Berik *et al*., 2010). For this purpose, each actuator row was assembled from three d_{15}-shear PIC255 patches of dimensions 25x25x0.5mm^3; the redesigned direct torsion actuator is shown in Figure 4b. In practice, the patches of each row have to be electrically wired in parallel since they have SP, while the two rows have to be wired in series since they are in OP. The experimentally reached maximum actuation voltage was 198V only, leading to a maximum actuation electric field of 396V/mm.

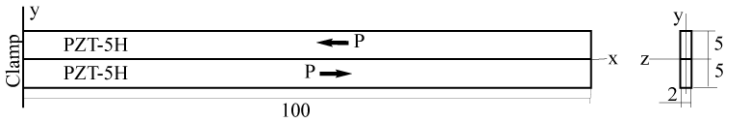

(a) *Theoretical torsion actuator (mm dimensions, in scale, Butz et al., 2008)*

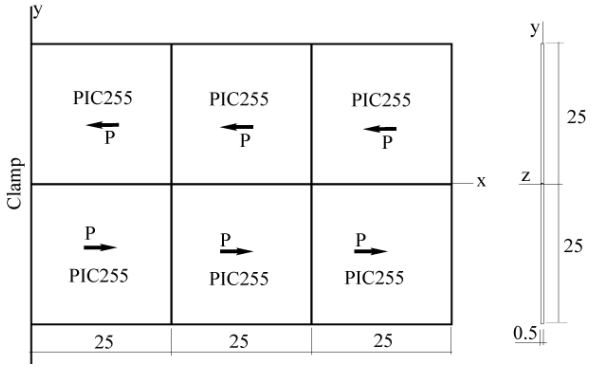

(b) *Present basic torsion actuator (mm dimensions, in scale, Berik et al., 2010)*

Figure 4. *Theoretical (a) and present (b) basic torsion actuators*

The proposed direct torsion actuator is here assessed using 3D FE analysis with ABAQUS® commercial code. Focus is made on the bonds and segmentation effects on the actuator behaviour and performance; for this purpose, the TRESCA stress criterion and transverse displacement distributions are analyzed with specific attention to the ranges and severity of the critical zones, that are expected to be mainly located at the rows and patches interfaces.

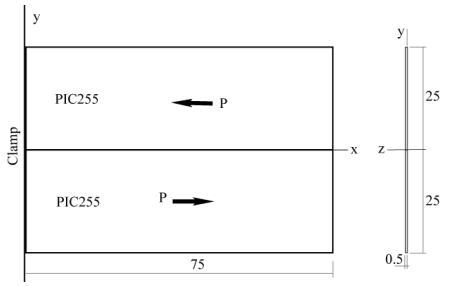

(a) *Basic model (without bond, mm dimensions, in scale)*

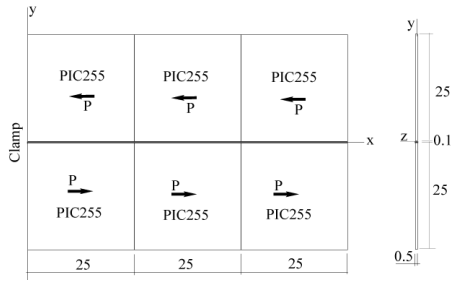

(b) *Six-patches actuator with inter-rows bond*

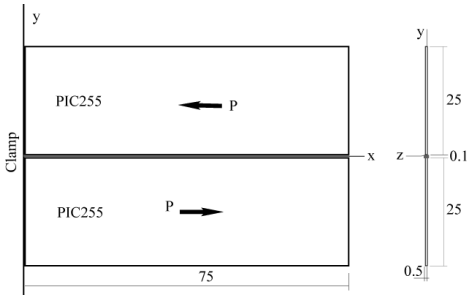

(c) *Enhanced model (with inter-rows bond)*

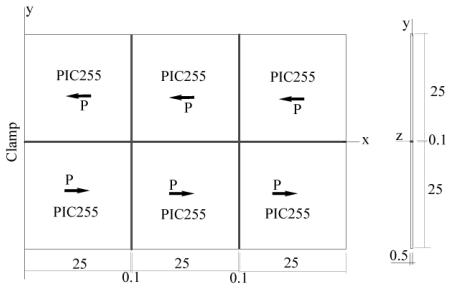

(d) *Detailed model (with inter-patches bonds)*

Figure 5. *The present basic torsion actuator analyzed models*

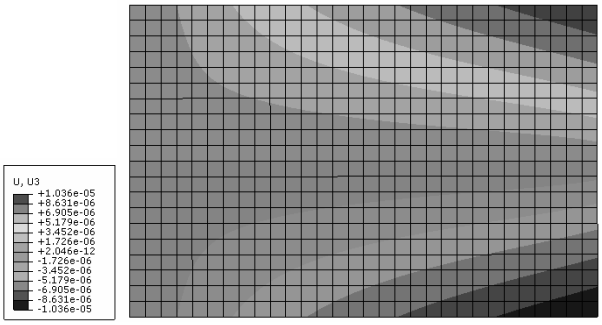

(a) *Basic model*

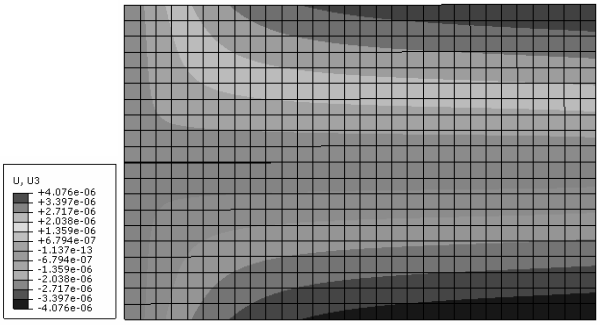

(b) *Enhanced model*

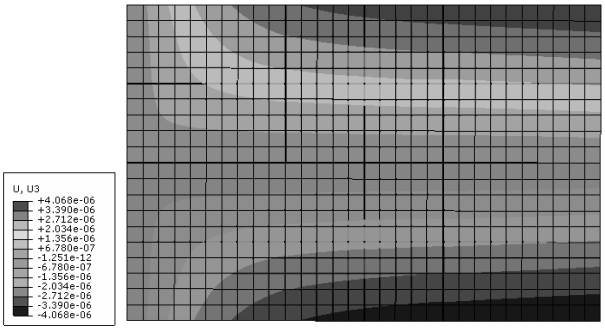

(c) *Detailed model*

Figure 6. *Present basic torsion actuator transverse displacement distributions*

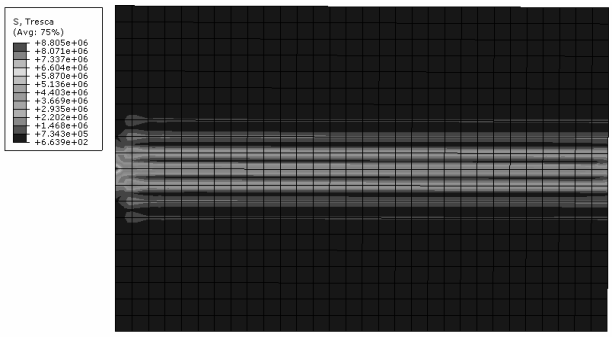

(a) *Basic model*

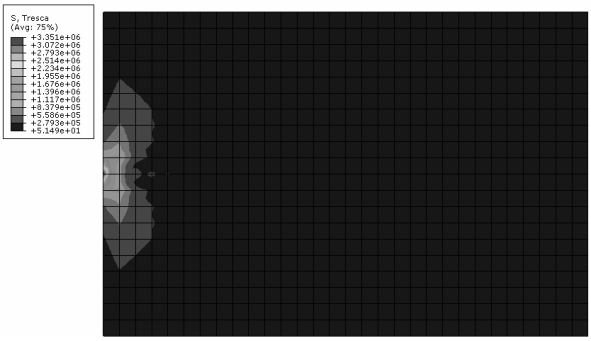

(b) *Enhanced model*

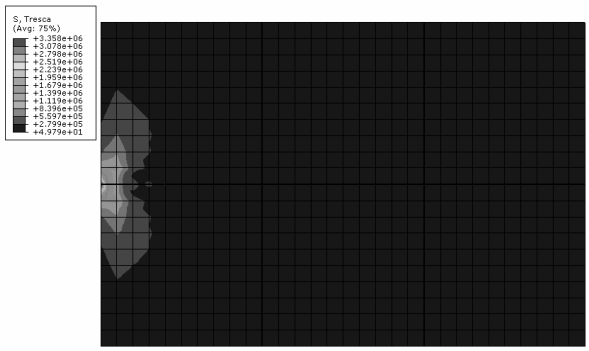

(c) *Detailed model*

Figure 7. *Present basic torsion actuator TRESCA stress distributions*

Different models are considered with increasing complexity. An obvious simplification consists in neglecting all bonds; since the patches of each row are in this case in perfect contact, they can be modelled as a single long patch as in Figure 5a; this represents the *basic model*. Each row is meshed with 30, 20 and 2 quadratic hexahedral piezoelectric FE (C3D20RE) along its length (x), height (y) and thickness (z), leading to an actuator total mesh of 2400 FE. A better assumption consists in neglecting only the inter-patches bonds, as in Figure 5b, leading to the *enhanced model* of Figure 5c. Here, the previous mesh is augmented by 30x1x2 quadratic hexahedral elastic FE (C3D20R) for the inter-rows bond. Finally, the *detailed model*, in the sense that it considers all bonds and the rows segmentations, is shown in Figure 5d.

Now, each patch has a mesh of 10x10x2 C3D20RE FE and the bond interfaces thickness is meshed with 1 C3D20R elastic FE and their meshes along the other directions should be the same as the neighbours patches ones in order to guarantee inter-patches and inter-rows mesh compatibility, thus the simulation convergence to the right solution. The OP is implemented by attaching local coordinate systems (*Csys Datum*) with opposite z-axes along the actuator length as shown in Figure 2. Materials properties are as listed in the Appendix.

Figures 6, 7 show, respectively, the transverse displacement and TRESCA stress distributions, while Table 1 shows their maximum values under a 198V actuation. They indicate that inter-rows bond reduces significantly the transverse deflection and stress criteria; besides, the shear stress concentration is greatly reduced and localized in a small zone at the actuator clamp (see Figure 7). They show also that inter-patches bonds, hence the rows segmentations, have only marginal effect on these criteria (compare distributions (b) and (c) of figures 6, 7, and values of the last two lines of Table 1) and can be dropped. Hence, in the following, only the basic and enhanced models will be used as cores of the smart composite sandwich. Table 1 confirms that the TRESCA stress criterion is the suitable dimensioning one here.

Table 1. *Torsion actuator maximum displacements and stress criteria under 198 V*

Criterion	Deflection (μm) and displacements ratios				Stress component/criteria (MPa)		
Model	U_3	U_3/U_1	U_3/U_2	U_2/U_1	Component	MISES	TRESCA
Basic	10.36	143.47	59.99	2.39	$\sigma_{13} = 4.374$	7.629	8.805
Enhanced	4.076	73.60	86.50	0.85	$\sigma_{33} = 5.475$	2.995	3.351
Detailed	4.068	73.43	86.52	0.85	$\sigma_{33} = 5.473$	3.000	3.358

Since the actuator axial displacement contains the warping information, the other cross-section displacement components values are normalized with its value and shown in Table 1 in order to assess the importance of the actuator warping. Table 1 shows that the warping effect can be neglected for the basic model but probably not for the other two models for which the adhesives presence seams to increase it; in fact,

the axial displacement is higher than the width one when the adhesives are considered (see enhanced and detailed models ratios of Table 1). On the other hand, as shown in the right part of Table 1, the adhesives seem to increase the normal transverse stress σ_{33} which dominates the other stress tensor components, unlike the basic model which is dominated by the transverse shear stress σ_{13}. These results will be checked next for the composite actuator.

4. Assessment of the composite actuator

The recent experimentally proved smart direct torsion actuator (Berik *et al*., 2010) is shown in Figure 8a; it consists of two identical glass fibre-reinforced plastic (GFRP) composite plates of length, height and thickness dimensions of 75x50x0.49mm^3, and elastic properties as given in the Appendix, that adhesively sandwich the six patch-assembled core torsion actuator of Figure 4b. Due to the thinness of the patches, no adhesives are put between them; however, they can get them from those bonding the faces to the core. Therefore, three models are considered: (i) a *sandwich model* resulting from y-z plane cuttings of an extruded block of dimensions 75x50x1.48mm^3; the same 30x20x2 mesh as for the core is used for each face, that has to be oriented locally along the global coordinate system, leading to a total mesh size of 30x20x(2+2+2)=3600 FE (Figure 8b). (ii) A *laminate model* resulting from adding 0.1mm-thick inter-layers (faces – core interfaces) bonds; it is constructed from y-z plane cuttings of an extruded single block of dimensions 75x50x1.68mm^3 (Figure 8c); each adhesive layer has a mesh of 30x20x1 FE, leading to a total mesh size of 30x20x(2+1+2+1+2)=4800 FE (Figure 8d). (iii) An *enhanced laminate model* is obtained by considering also a 0.1mm-thick inter-rows (core rows interface) bond; it results from extruding along the positive and negative z-axis, as in Figure 8e, all domains of the enhanced model shown in Figure 5c. Here also, each face and core are meshed with 2 FE, and each bond thickness has 1 FE; this leads to a total mesh of 30 x (20+1) x (2+1+2+1+2)=5040 FE.

Figures 9, 10 show, respectively, the transverse displacement and TRESCA stress distributions under a 198V actuation. Figure 9 indicates that the transverse displacement distribution is marginally affected by the adhesives for the three FE models; it corresponds to that of the basic model of the core (see Figure 6a). However, Table 2, which gives above criteria maximum values under a 198V actuation, shows that the transverse displacement values decrease with increasing the bonds number. Regarding the TRESCA stress distributions (Figure 10), they are similar to those of the core basic model (Figure 7a) for the first two models; their values, as given in Table 2, are marginally affected by the inter-layer adhesives, but divided by more than two due to the core inter-rows bond. The comparison with the measured maximum deflection at 198V (5.267μm given in Berik *et al*. 2010) proves (see Table 2) that the most accurate analyzed model is the enhanced laminated one (within -4.08% error) which considers both inter-layers and inter-rows adhesives.

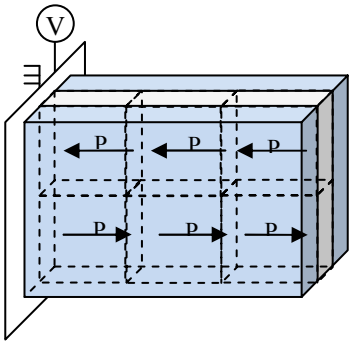

(a) *Tested composite torsion actuator (Berik et al., 2010)*

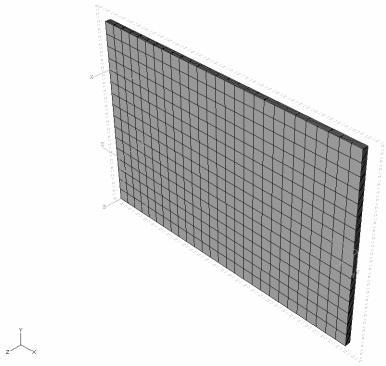

(b) *Sandwich FE model*

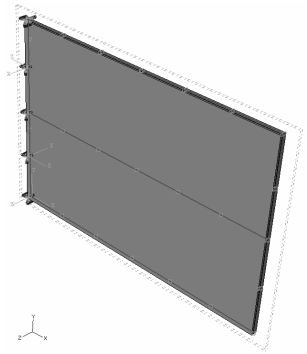

(c) *Laminate CAD model*

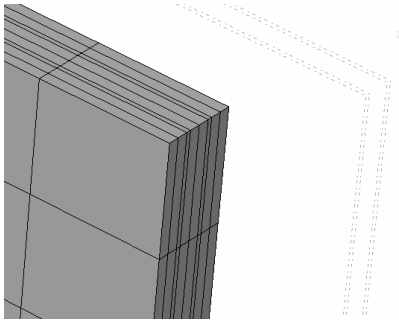

(d) *Laminate FE model (thickness zoomed)*

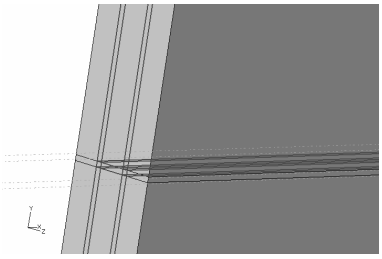

(e) *Enhanced laminate CAD model (interfaces zoomed)*

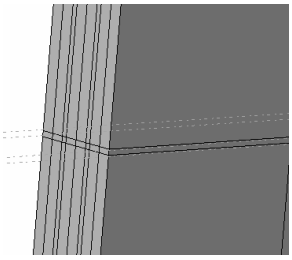

(f) *Enhanced laminate FE model (rows interface zoomed)*

Figure 8. *Tested composite torsion actuator (a) CAD (c,e) FE models (b,d,f)*

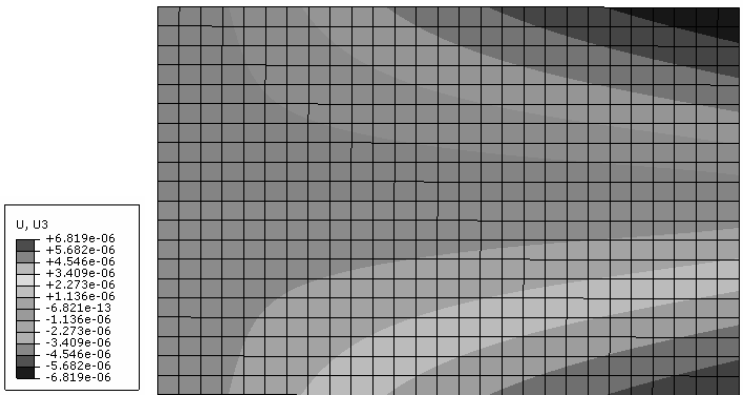

(a) *Sandwich model*

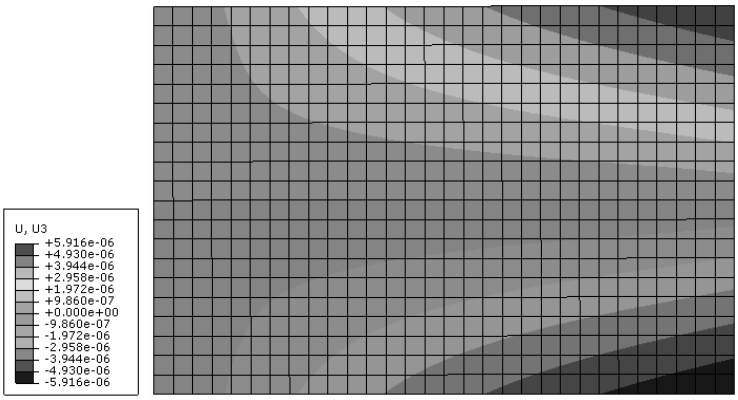

(b) *Laminate model*

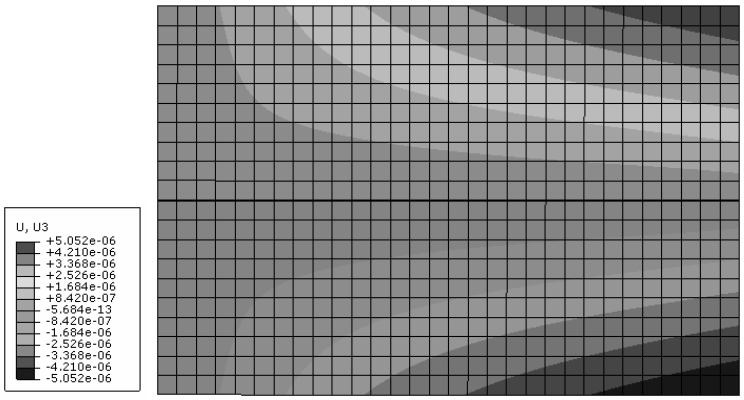

(c) *Enhanced laminate model*

Figure 9. *Tested composite torsion actuator transverse displacement distributions*

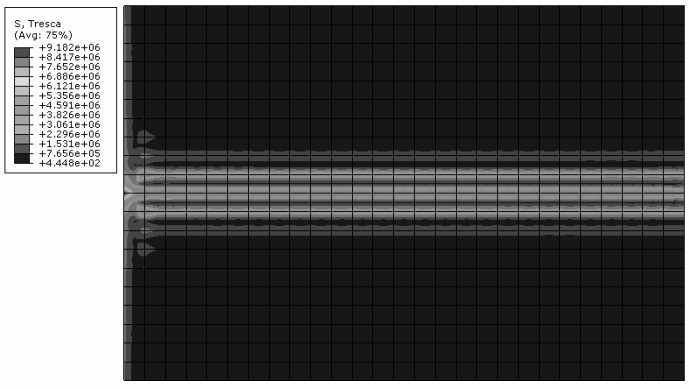

(a) *Sandwich model*

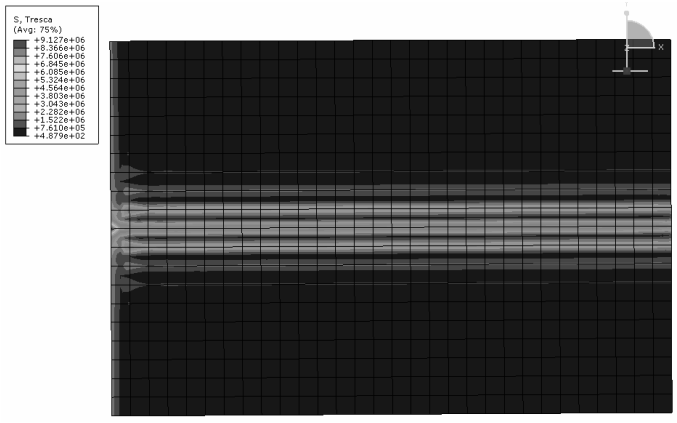

(b) *Laminate model*

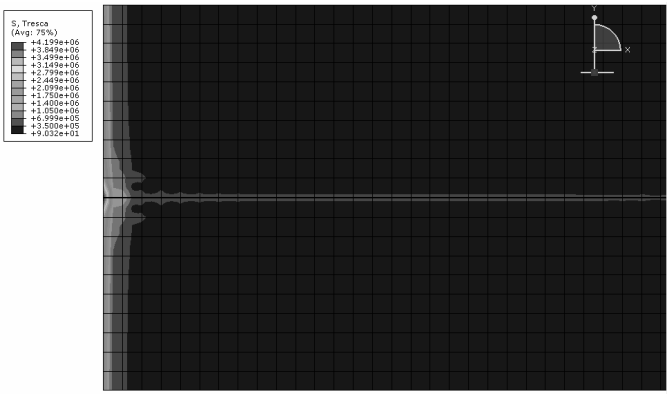

(c) *Enhanced laminate model*

Figure 10. *Tested torsion actuator TRESCA stress distributions*

Table 2. *Composite torsion actuator models maximum displacements and stress criteria under 198 V actuation. Values between brackets indicate errors with respect to the experimental reference value (5.267 μm as given in Berik et al. 2010)*

Criterion	Deflection (μm) and displacements ratios				Stress component/criteria (MPa)		
Model	U_3	U_3/U_1	U_3/U_2	U_2/U_1	Component	MISES	TRESCA
Sandwich	6.819 (+29.47%)	98.597	23.893	4.127	$\sigma_{13} = 4.587$	7.952	9.182
Laminate	5.916 (+12.32%)	81.962	21.474	3.817	$\sigma_{13} = 4.559$	7.904	9.127
Enhanced laminate	5.052 (-4.08%)	86.759	22.003	3.943	$\sigma_{33} = 6.119$	3.706	4.199

As for the basic torsion actuator (see Table 1), the other cross-section displacement components values are normalized with respect to the axial value and given in Table 2 in order to assess the importance of the actuator warping. Table 2 shows that the width displacement is now much higher, than that of the basic torsion actuator, for the three models independently of the presence of the adhesives (see corresponding columns of Table 2); the axial displacement is now around 4 times lower than the width one. Nevertheless, it is thought that the warping could be present but may be low. On the other hand, as shown on the right part of Table 2, the inter-layers adhesive has marginal effect, while the inter-rows one increases the normal transverse stress σ_{33} which dominates the other stress tensor components, unlike the other two models which are dominated by the transverse shear stress σ_{13}. Here also, the TRESCA stress criterion appears to be the suitable dimensioning one.

From Table 2 and the comparison with the experimental result, it can be concluded that the inter-rows adhesive is more influential than the inter-layers one. It has stiffened the torsion actuator so that its integrity should be enhanced since the stress criteria were more than divided by two in this case (see the lower right part of Table 2); but, this advantage is compensated by the transverse deflection performance reduction (see lower left part last line of Table 2).

5. Open-circuit modal analysis

Piezoelectric actuators are generally used in dynamic applications. It is then very important to run the basic and composite torsion actuators modal analyses in order to identify the torsion modal shape that compares with the static torsion actuation-induced deformed shape. Another objective of the following modal analysis is to assess the adhesives, or models refinements, on the modal parameters, in particular, for the targeted torsion mode. Only OC electric conditions are considered since they ensure the presence of the piezoelectric stiffening effect (Benjeddou 2009); the

equipotential and OC conditions were imposed on the +z electrode, while the other one was considered grounded. Since the patches segmentation was not found influential on the basic torsion actuator performance indicators, the corresponding (detailed) model is not considered in the following modal analyses. Also, the first four modal shapes were found to be the same for the four models; hence, they are shown here (superposed to the non deformed shapes) only for the first (basic) torsion actuator model. The (m,n) values, shown in Figure 11 and used for its text comments, indicate (x,y) axes zero crossing numbers; they serve for easy nomenclature and classification of the modal shapes.

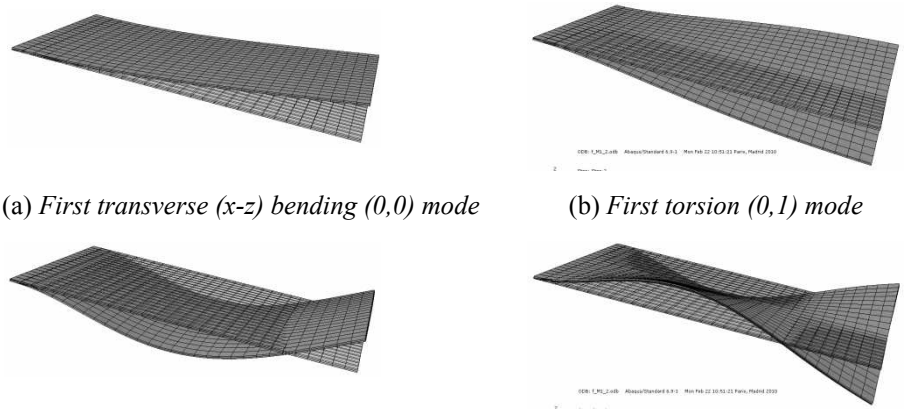

(a) *First transverse (x-z) bending (0,0) mode* (b) *First torsion (0,1) mode*

(c) *Second transverse (x-z) bending (1,0) mode* (d) *Second torsion (1,1) mode*

Figure 11. *The torsion actuator basic model first (four) OC modal shapes*

Figure 11 indicates that the first and third modes are the lengthwise fundamental (0,0) and second (1,0) bending plane (x-z) beam-like modes, while the second and fourth modes are the targeted (see Figure 3) first (0,1) and the second (1,1) torsion modes. It is then the former that is similar to the static deformation under 198V direct torsion actuation as given in Figure 3. So, it is the first torsion mode frequency that should be targeted for dynamic applications.

The frequencies of the first OC modes are provided in Table 3. From the latter it can be noticed that inter-rows adhesive lowers strongly its modal frequencies; this is due mainly to the softening effect of this adhesive. On the other hand, sandwiching the torsion actuator with the composite faces raises its modal frequencies; this is due to the faces stiffening effect on the core. The last two columns of Table 3 show also that the inter-layers adhesive raises the modal frequencies, while the inter-rows one decreases them as for the basic torsion actuator. It can then be concluded that the composite faces stiffen the torsion actuator, while the adhesives act oppositely, in the sense that the inter-layers adhesive stiffens it, while the inter-rows one softens it.

Table 3. *Basic and composite torsion actuators first (four) OC frequencies (Hz)*

FE Models			Basic actuator		Composite actuator		
Order	(m,n)	mode type	Basic	Enhanced	Sandwich	Laminate	Enhanced
1	(0,0)	1st x-z bending	2694.7	37.381	120.46	139. 51	139.55
2	(0,1)	1st torsion	9640.5	133.56	256.71	290.80	289.95
3	(1,0)	2nd x-z bending	16 650	231.33	748.36	859.93	859.16
4	(1,1)	2nd torsion	32 227	446.45	985.99	1118.40	1115.20

6. Bonding parametric analysis

As the adhesive was found to be very influential on the torsion actuator behaviour and performance, and since its geometric and material properties are not precisely known, a parametric analysis was conducted by varying separately the laminate inter-layers adhesive thickness and elastic constants; the adhesive is assumed elastically isotropic; hence, its Young's modulus and Poisson's ratio were varied separately, and the shear modulus influence is just post-treated from them using G=E/[2(1+ν)]. The adhesive properties are also given in the Appendix.

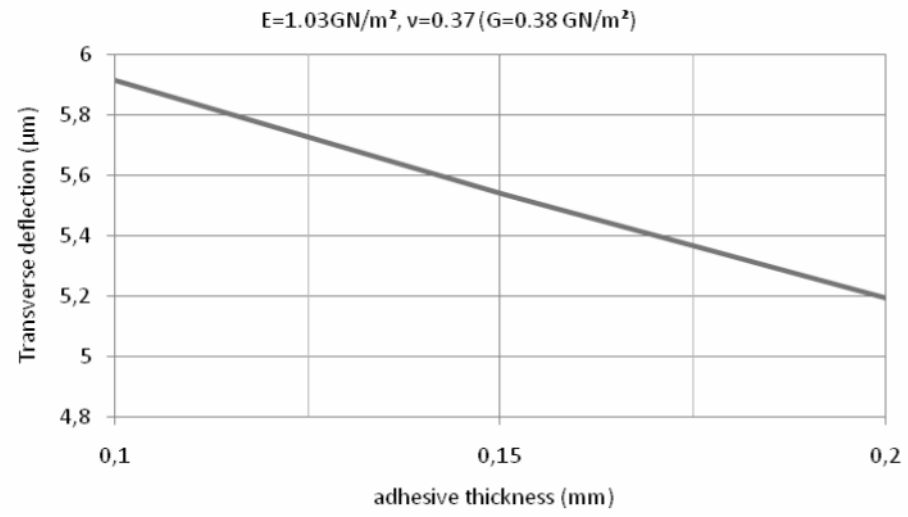

Figure 12. *The torsion actuator laminate model deflection under 198V static torsion actuation for varied adhesive thickness (axes values commas should be read dots)*

The influence of the inter-layers adhesive thickness on the torsion actuator transverse displacement under 198V actuation voltage is shown in Figure 12; the latter shows that, as expected, the increase of the adhesive thickness stiffens the actuator since the latter's transverse deflection decreases by 12.12% after doubling the adhesive thickness.

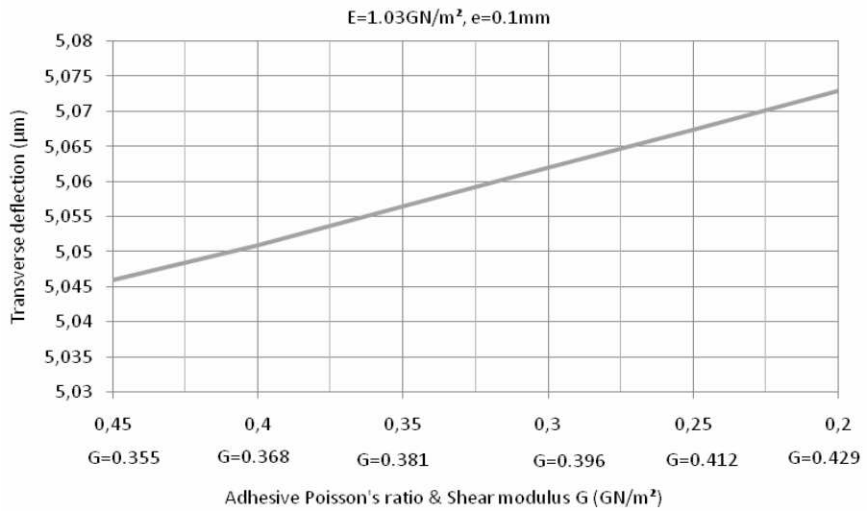

Figure 13. *The torsion actuator laminate model deflection under 198V static torsion actuation for varied adhesive Poisson's ratio (axes values commas should be read dots)*

The influence of the laminate inter-layers adhesive Poisson's ratio on the composite torsion actuator transverse displacement under 198V actuation voltage is shown in Figure 13; the latter shows that, as expected, the Poisson's ratio softens slightly the actuator since the latter's transverse deflection increases by only 0.56% with decreasing by more than half (55.56%) the adhesive Poisson's ratio.

The influence of the laminate inter-layers adhesive Young's modulus on the composite torsion actuator transverse displacement under 198V actuation voltage is shown in Figure 14 for two adhesive thickness values and for a Poisson's ratio of ν=0.37. It is clear that the Young's modulus has marginal stiffening effect (see the lower curve for the thicker adhesive) on the actuator performance.

The influence of the laminate inter-layers adhesive shear's modulus on the composite torsion actuator transverse displacement under 198V actuation voltage is shown in Figure 15. It is clear that the shear modulus has a moderate softening effect on the actuator since doubling the shear modulus (increase by 94.15%) increases the actuator transverse deflection by 9.54%.

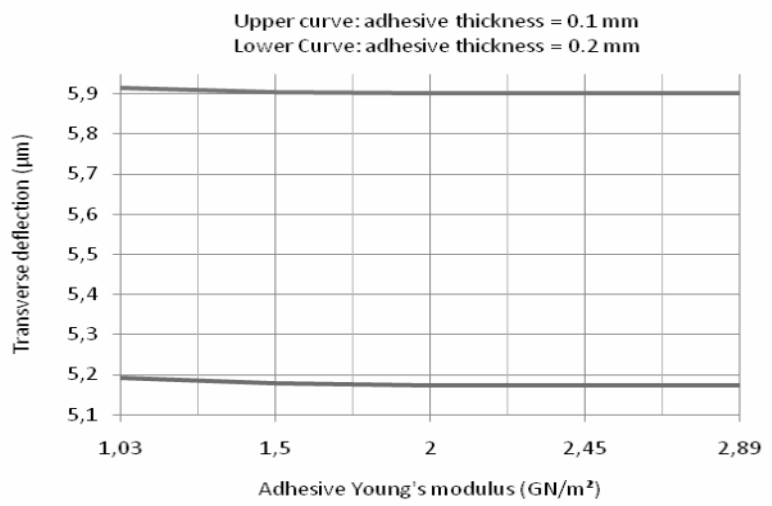

Figure 14. *The torsion actuator laminate model deflection under 198V static torsion actuation for varied adhesive Young's modulus and thickness (axes values commas should be read dots). ν=0.37*

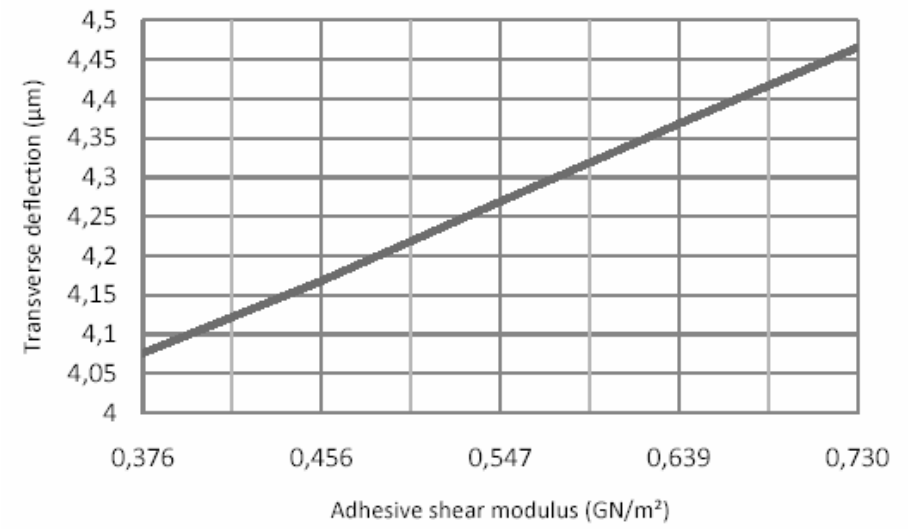

Figure 15. *The torsion actuator enhanced laminate model deflection under 198V static torsion actuation for varied adhesive shear modulus (axes values commas should be read dots)*

This parametric analysis shows that, as expected, the most influential parameters of the laminate inter-layers adhesive bond on the composite torsion actuator are its thickness and shear modulus; the latter combines the effects of the Poisson's ratio and Young's modulus.

7. Conclusions and perspectives

A recently experimentally proved direct torsion actuation smart concept has been here numerically assessed using 3D finite element analysis by ABAQUS® commercial code in order to avoid any kinematics assumptions influence. The torsion actuator core assessment, regarding the effects of the inter-rows bond and segmentation (with inter-patches bonds), has shown that only the former is influential on the actuator behaviour and performance. Then, the smart composite actuator assessment indicates that a realistic FE model, from the three considered ones, should consider both inter-layers and inter-rows bonds. Moreover, the conducted open-circuit modal analysis confirms that the inter-rows adhesive softens the actuator while the inter-layers one stiffens it. The composite faces have not only a protective role, but also an integrity enhancement function. Besides, the conducted parametric analysis indicates that, as expected, the most influential parameters of the laminate inter-layers adhesive on the composite actuator behaviour and performance are its thickness and shear modulus.

As a perspective of this work, the present modal analysis can be experimentally validated, and that of the detailed model, considering the adhesives between the vertical interfaces of the patches, can be simulated and its influence could be analysed in comparison to the eventually run tests; the individual patches electrodes are expected to affect the resulting modal effective electromechanical coupling coefficient indicator. Other perspectives include the validation of the present parametric analysis by numerical plans of experiments and its extension to other parameters like the number of used patches and their dimensions within the available ones, and the development of an analytical solution to conduct an analytical sensitivity analysis of the composite direct torsion actuator performance with regards to the influencing parameters that were revealed here or with regards to some additional ones that have not been considered here but mentioned above.

Acknowledgements

The author greatly appreciates the financial support of the Austrian Centre of Competence on Mechatronics (ACCM) at Linz (Austria), through the international scientific partnership contract (1st July 2010 – 31st December 2012) on research area 2 (Mechanics and Model-based Control of Structures and Machines) co-coordinated by Dr. M. Krommer from the Institute of Technical Mechanics, headed by Prof. H. Irschick, of the Johannes Kepler University at Linz (Austria). Dr.

Krommer and Prof. Irschick are also sincerely thanked for their fruitful cooperation on this manuscript subject. Finally, the author's thank goes to his student, Miss V. Rouzier, for some of the presented figures and tabulated values that were obtained under the author supervision.

8. References

Benjeddou A., "Shear-mode piezoceramic advanced materials and structures", *Mechanics of Advanced Materials and Structures*, vol. 14, n° 4, 2007, p. 263-275.

Benjeddou A., "New insights in piezoelectric free-vibrations using simplified modeling analyses", *Smart Structures and Systems*, vol. 5, n° 6, 2009, p. 591-612.

Berik P., Benjeddou A., "Piezoelectric d_{15} shear response-based torsion actuation mechanism: an experimental benchmark and its 3D finite element simulation", *International Journal of Smart and Nano Materials*, vol. 1, n° 3, 2010, p. 224-235.

Butz A., Klinkel S., Wagner W., "A geometrically and materially non-linear piezoelectric three-dimensional beam finite element formulation including warping effects", *International Journal for Numerical Methods in Engineering*, vol. 76, n° 5, 2008, p. 601-635.

Centolanza L. R., Smith E. C., Munsky B., "Induced-shear piezoelectric actuators for rotor blade trailing edge flaps", *Smart Materials and Structures*, vol. 11, n° 1, 2002, p. 24-35.

Chevallier G., Ghorbel S., Benjeddou A., "A benchmark for free-vibration and effective coupling of thick smart structures", *Smart Materials and Structures*, vol. 17, n° 6 (065007), 2008.

Chevallier G., Ghorbel S., Benjeddou A., "Piezoceramic shunted damping concept: testing, modelling and correlation", *Mécanique & Industrie*, vol. 10, n° 5, 2009, p. 397-411.

Chopra I., "Review of state of art of smart structures and intelligent systems", *AIAA Journal* vol. 40, n° 11, 2002, p. 263-275.

IEEE Inc., *Standard on Piezoelectricity*, ANS/IEEE Std 176-1987, 1988.

Powar O. M., Jung S. N., "Single-crystal-material-based induced-shear actuation for vibration reduction of helicopters with composite rotor systems", *Smart Materials and Structures*, vol. 17 (065009), 2008.

Thakkar D., Ganguli R., "Helicopter vibration reduction in forward flight with induced-shear based piezoceramic actuation", *Smart Materials and Structures*, vol. 13, 2004, p. 599-608.

Tzou H. S., Ye R., Ding J. H., "A new X-actuator design for dual bending/twisting control of wing", *Journal of Sound and Vibration*, vol. 82, 2008, p. 836-846.

Zehetner C., "Compensation of torsional vibrations in rods by piezoelectric actuation", *Acta Mechanica*, vol. 207, 2009, p. 121-133.

9. Appendix

Table 4. *Materials data used for the present finite element simulations*

Materials	Constants	Notations	Values
Core's PIC255 piezoceramic patches (Data from PI Germany given for standard 3-axis or thickness poling)	Piezoceramic stress constants (C/m^2)	$e_{31}=e_{32}$	-7.15
		e_{33}	13.7
		$e_{15}=e_{24}$	11.9
	Permittivity constants at constant strain (nF/m)	$\in_{11}^{S}=\in_{22}^{S}$	8.234
		$\in_{33}^{S}$	7.588
	Young's modules (GN/m^2)	$E_1=E_2$	62.89
		E_3	47.69
	Shear modules (GN/m^2)	G_{12}	23.15
		$G_{13}=G_{23}$	22.26
	Poisson's ratios	ν_{12}	0.36
		$\nu_{13}=\nu_{23}$	0.46
	Mass density (Kg/m^3)	ρ	7800
G-EV- 760R Glass Fiber/Epoxy composite faces	Young's modules (GN/m^2)	E_1	33.11
		$E_2=E_3$	13.1
	Shear modules (GN/m^2)	$G_{12}=G_{13}$	3.0
		G_{23}	2.3
	Poisson's ratios	$\nu_{12}=\nu_{13}$	0.27
		ν_{23}	0.40
	Mass density (Kg/m^3)	ρ	2500
Two-component Adhesive bonding	Young's modulus (GN/m^2)	E	1.03
	Poisson's ratio	ν	0.37
	Mass density (Kg/m^3)	ρ	1000